Mon. Not. R. Astron. Soc. **000**, 000–000 (0000) Printed 1 February 2008 (MN LATEX style file v1.4)

Molecular and Ionised Gas Motions in the Compact HII region G29.96–0.02

S.L. Lumsden[1] and M.G. Hoare[2]

[1] Anglo-Australian Observatory, PO Box 296, Epping, NSW 1710, Australia – sll@aaoepp.aao.gov.au
[2] Department of Physics and Astronomy, University of Leeds, Leeds LS2 9JT, UK – mgh@ast.leeds.ac.uk

arXiv:astro-ph/9901196v1 15 Jan 1999

1 February 2008

ABSTRACT

We present a new observation of the compact HII region, G29.96−0.02, that allows us to compare the velocity structure in the ionised gas and surrounding molecular gas directly. This allows us to remove most of the remaining ambiguity about the nature of this source. In particular, the comparison of the velocity structure present in the $4^{1,3}$S–$3^{1,3}$P HeI lines with that found in the 1–0 S(1) H_2 line convincingly rules out a bow shock as being important to the kinematics of this source. Our new observation therefore agrees with our previous conclusion, drawn from a velocity resolved HI Brγ map, that most of the velocity structure in G29.96−0.02 can largely be explained as a result of a champagne flow model. We also find that the best simple model must invoke a powerful stellar wind to evacuate the 'head' of the cometary HII region of ionised gas. However, residual differences between model and data tend to indicate that no single simple model can adequately explain all the observed features.

Key words: H II regions - interstellar medium: kinematics and dynamics - interstellar medium: individual(G29.96-0.02)

1 INTRODUCTION

The study of ultracompact (UC) H II regions has been stimulated in recent years by the sparsely sampled VLA survey of Wood & Churchwell (1989). One of the greatest puzzles of the Wood & Churchwell survey is the total number of such regions found. By taking both the total number of O stars in the galaxy (simply from extrapolating the number of optically visible OB associations), and their lifetimes on the main sequence, they predicted the total number of such sources that might still be expected to be in the UC H II phase. Comparing this with the numbers actually found led Wood & Churchwell to conclude that there was an order of magnitude more sources in their VLA survey than there should have been. Since there is no other evidence for the massive star formation rate being this much larger than expected, they considered that the likeliest solution to this problem is that some mechanism is constraining the outward expansion of the H II region. Wood & Churchwell estimate that the UC H II phase must last about ten times longer than the $\sim 10^4$ years predicted on the basis of simple Strömgren sphere expansion. Another key result from the Wood & Churchwell study is that at least 20% of these regions have a 'cometary' appearance. A subsequent survey by Kurtz et al. (1994) and a VLA survey of much larger, optically visible, H II regions by Fich (1993) also found a similar proportion of this type.

These discoveries stimulated interest in the study of new models for the evolution of compact HII regions. Some of the key models that have been developed recently that can explain the lifetime of the compact HII regions can be summarised as follows:

• Bow shock models: The near parabolic shape of many of these sources lead Wood & Churchwell to develop a bow-shock interpretation for UC H II regions which provides an explanation for both of the lifetime and the cometary morphologies. The basis of this model is that an OB star moves supersonically through a molecular cloud ($v_* > 0.2$ kms^{-1}) and the stellar wind from the star supports a bow shock along its direction of motion (Mac-Low et al. 1991, Van Buren & Mac-Low 1992). This shock can trap the ionisation front (IF), preventing it from expanding and the lifetime of the UC H II phase in this model is simply the star's crossing time through the cloud, typically of the order of 10^5 years.

• Mass loading models: Dyson and co-workers (Dyson et al. 1995; Redman et al. 1996) have investigated the interaction of a stellar wind and a clumpy molecular cloud material. This provides a source of fresh neutral material to soak up ionising photons which is an efficient mechanism for slowing the expansion. A density gradient of mass-loading clumps can also account for the cometary regions (Williams et al. 1996, Redman et al. 1998). Lizano et al. (1996) offer

© 0000 RAS

a slightly different perspective on the same process. Hollenbach et al. (1994) invoked photoevaporation of a disk around the exciting star itself to feed material, but this does not help to account for the known morphologies.

• 'Environmental' models: De Pree, Rodriguez & Goss (1995) suggested that there was evidence that the ambient density in the natal molecular clouds was much higher than assumed in traditional Strömgren sphere expansion arguments. In a sense this 'model' argues that there is in fact no problem, rather that Wood & Churchwell used inaccurate parameters in calculating the expected growth rates of the HII regions initially. In this picture the likeliest explanation for the observed fraction of compact HII regions that appear 'cometary' is given by the champagne flow model described next.

• Champagne flow (blister) models: HII regions with cometary morphology were originally labelled as 'blisters' by Israel (1978) because of their propensity for being found near the edges of molecular clouds (the classical example being the Orion nebula itself of course). Icke, Gatley & Israel (1980) noted that if there is a density gradient in the ambient gas the H II region will expand fastest in the low density direction and so become very asymmetric. Tenorio-Tagle and co-workers in a series of papers (see Yorke et al. 1983 for a summary) developed numerical models of the evolution of HII regions for this asymmetric expansion. They found that the pressure gradient set up when the IF reaches the edge of the cloud causes a 'champagne' flow of ionized gas away from the cloud with velocities of order 30 kms^{-1}. Although in its original form this model does not answer the lifetime problem, it may when combined with either higher ambient densities, stellar wind trapping of the ionization front or mass loading.

Whilst it is clear from the above that no single observational test can absolutely prove that one of these models is correct, the velocity structure within the ionised and molecular gas provides a key discriminating test. Previous attempts to study the molecular gas in the mm regime have turned up unexpected results. Hot ammonia clumps (Cesaroni et al. 1994) and water masers (Hofner & Churchwell 1996) often appear to be more associated with a subsequent generation of star formation rather than probing the adjacent molecular gas. Observations of tracers of the more quiescent gas such as CO have mostly been made with low spatial resolution and optical depth and excitation effects can also make interpretation difficult.

G29.96–0.02 is perhaps the best studied of the compact cometary sources for which evidence of a bow shock has been found. Wood & Churchwell (1991) carried out high resolution radio recombination line studies, and the results were analysed by Van Buren & Mac Low (1992), who claim good agreement with their bow-shock model. We showed in a previous paper (Lumsden & Hoare 1996: hereafter LH96) however, that their conclusions were biased because of the low sensitivity to extended structure in their data. By mapping the HI Brγ line we instead found much better agreement with a model that had a strong champagne flow component. In this paper we present new data, allowing us to tie the motions in the molecular and ionised gas together without ambiguity for the first time.

2 OBSERVATIONS

We obtained high resolution ($R \sim 20000$) spectra of the 1–0 S(1) H_2 line with the common user IR array spectrometer CGS4 on UKIRT on the night of 4 July 1997. We used the echelle grating within CGS4, with a one pixel wide slit (each pixel corresponding to $1.0''$ in the dispersion direction and $1.5''$ along the slit). The effective resolution of this combination was measured to be 18 ± 1 kms^{-1} on several bright OH night sky lines (intrinsic width assumed to be $\ll 10\mathrm{kms}^{-1}$), and from a krypton arc lamp. To fully sample the resolution element, the array was stepped six times across two pixels. This oversampling is extremely useful in determining accurate line profiles for our data. The slit was set at a position angle of 60°, in order to be approximately along the symmetry axis of G29.96−0.02.

Our basic observing technique was to observe at each position for ten minutes (composed of five two minute exposures), and then take a separate two minute sky frame. Since the night sky lines are well separated from the emission lines in our target we do not need to achieve a good cancellation of these. The separate sky frame acts as a dark frame to remove dark current from the array more than to subtract the night sky emission. We coadded five such data blocks (ie total time per position on source was 50 minutes). We observed three positions in total, aligned with the peak flux from the object and 6 arcseconds northwest and southeast of this. Our data can be compared directly with the equivalent HI Brγ data from LH96.

The most crucial part of the data reduction is accurate wavelength calibration since we wish to compare the relative velocities of the observed lines directly. Unfortunately, flexure can give rise to significant wavelength shifts in CGS4, so it is not feasible to use arc lamps to calibrate the wavelength scale. Instead, we derived a wavelength calibration using the actual night sky lines on the frame. This ensures that we are not affected by the flexure problems, since the calibration is now self consistent with the emission line data: it does however mean that the absolute reference for the velocity is only as accurate as the night sky emission lines. Each frame was shifted onto a constant wavelength scale before the co-addition into the final three images. In addition to the correction for flexure (which appears as a bulk wavelength shift for all slit positions), the projection of the slit onto the array is curved. We also corrected for this curvature. We tested for residual errors in these corrections by measuring wavelengths of night sky lines in different frames and at different positions along the slit. We are confident that the residual errors in the measured relative velocities due to these corrections are $< 1\mathrm{kms}^{-1}$.

For the OH lines, we used the tabulated wavelengths given in Oliva & Origlia (1992), and allowed for the splitting of the doublets (since this leads to resolvable lines in some instances). With the 256×256 array now used in CGS4, the wavelength coverage ($\sim 0.027\mu$m), allowed us to observe 11 identifiable lines. We were able to derive a very good fit to the tabulated values, with a final rms error of $1.1 \times 10^{-5}\mu$m (or only $1.5\mathrm{kms}^{-1}$ in velocity terms). The best fit to CGS4 echelle data is quadratic in the estimated wavelength (note that this is different to our assumption in LH96 where we adopted a linear shift from the brightest arc or OH lines). Lastly, we corrected the observed velocities into standard

v_{LSR} values by correcting for the solar motion. We checked the derived dispersion correction for the spectrum using this method with that obtained from a krypton arc lamp. Although there was an offset because of flexure as already noted, the actual dispersion correction was very similar, giving us confidence in our adopted approach.

We now return briefly to the case of the absolute wavelength calibration of the Brγ data published in LH96. As part of a separate project we have obtained spectra of planetary nebulae (PN) with the same configuration. Of these ~ 10 are known to have accurate measured radial velocities. We used this information to derive a calibration from the OH night sky lines at Brγ as well (it was possible to apply this method since the PN data were also obtained with the larger array, whereas the original LH96 data were obtained using a smaller 58×62 device). Although the tabulated Oliva & Origlia values again gave a good dispersion correction, we found an offset between the PN data and the known radial velocities. We derived an average correction to apply, and then used this knowledge to derive a similar wavelength calibration for G29.96−0.02. The result is rather different to that given in LH96. For the pixel with the largest flux, we derive a velocity of 97.2kms^{-1}. We also carried out observations of a smaller set of PN to calibrate the error in the H_2 data. From this we derive the velocity of the pixel with the peak HeI intensity as 98.3kms^{-1}, in very good agreement with the HI line value. We also used the same PN data to estimate the relative error in the velocity scale between the HeI lines and H_2 data, and found an average difference of $\sim$ 2kms^{-1} assuming the H_2 and HeI trace the same structure in the PN. Therefore we assume that the overall scale of both datasets is accurate to $\pm$3kms^{-1} (which is also consistent with the derived errors in the actual arc fitting process for both datasets as well). We are however confident that there is no evidence for any difference in the absolute velocity of the HI and HeI from our data, and have therefore assumed that they are the same in what follows (ie we have normalized the data to have the same velocity for the point with the largest observed line flux in the ionised component).

Figure 1 shows the coadded spectrum of the region around the peak of the ionised emission. The lines evident are the $4^{3,1}$S–$3^{3,1}$P transitions of HeI, and the 1–0 S(1) transition of H_2. In comparing our data with the models we also require very accurate theoretical or measured wavelengths. The vacuum rest wavelength for the H_2 line was taken as 2.121833μm from Bragg, Brault & Smith (1982), whilst the values for the HeI lines were derived from energy levels in Bashkin & Stoner (1975) from which we found 2.113772μm and 2.112743/2.112657/2.112584μm for the singlet and triplet transitions respectively. For the singlet transition there is no ambiguity as to which spin state dominates the transition, and hence we know the exact line wavelength, though the singlet transition is of course weaker than the triplet. We therefore measured the actual observed wavelength difference between the singlet and triplet helium lines for all positions where the singlet line was easily detected, and calculated a weighted average. The result was a difference of $1.188\times10^{-3}\mu$m, consistent with the triplet line being dominated by transitions to the $J = 2$ state. Therefore, the expected wavelength difference between the triplet HeI line and the H_2 transition, assuming both components have the same velocity is $9.249\times10^{-3}\mu$m. Observed variations from this value of course represent different real velocity structures in the ionised and molecular gas.

Observations were also made of SAO142608, a B0 star with a visual magnitude of $V = 8.6$. There are only very weak atmospheric absorption lines present in the observed wavelength range, and none of these lie near the target emission lines. The data shown in Figure 1 have been crudely flux calibrated using this star, to allow relative fluxes from the HeI and H_2 lines to be estimated.

3 RESULTS

All data were fitted with Gaussian functions, there being no evidence for deviations from this profile within the errors. The actual results are shown in Figure 2, where we have plotted data for the H_2 line, the HeI triplet and the relevant Brγ data from LH96.

We have only plotted points where the signal to noise in the flux was greater than 4. Given our comments in the previous section we have taken the liberty of shifting the velocity scale for the Brγ and HeI so that they agree at the position of peak flux. The absolute scale adopted is the one derived from the HeI observations. In addition, it should be noted that the spatial resolution of the Brγ is less (2 arcsec pixels as opposed to the 1.5 arsec pixels for the new data presented here).

First, we compare the flux distributions of the molecular hydrogen emission and the He I and Brγ emission along the on-axis slit position (top-left panel of Fig 2). As expected the He I and Brγ distributions trace each other very well, but the molecular hydrogen emission peaks nearly 2 arcsec or about 0.05 pc ahead of the ionized gas away from the exciting star. The 1-0 S(1) distribution is also much flatter than the ionized gas in the main body of the nebula. Similar relative distributions are seen in the off-axis positions in Fig 2. This is consistent with the molecular hydrogen emission arising in a thin shell just outside the ionized region which would be predicted by both fluorescent and shock models.

In the middle panel of Fig 2 we compare the centroid velocity of the molecular hydrogen emission along the on-axis position with that of the He I and Brγ line. As expected the velocity structure of the He I is very similar to that of Brγ since they both trace the same volume of ionized gas. On the other hand the molecular hydrogen does show significantly different velocity structure. There is much less variation in the velocity along the object: only about 7 kms^{-1} in the molecular hydrogen compared to over 20 kms^{-1} for the ionized gas. The molecular velocity structure has the appearance of an approximately constant background emission at $v_{lsr} \approx$92 kms^{-1} with perturbations in the same direction as the ionized gas in the main body of the nebula. In the region around the exciting star (2 arcsec behind the nebular peak) the ionized gas is redshifted relative to the molecular gas by about 3 kms^{-1} whereas in the tail the ionized gas gets progressively more blueshifted relative to the molecular gas. In the head region the molecular gas again returns to the 'background' velocity whilst the ionized gas rapidly becomes more and more blueshifted. Similar patterns are again seen in the off-axis positions, especially in the 6 arcsec SE position where there is still significant velocity structure in the molecular hydrogen.

The comparison of the line widths is shown in the bottom panel of Fig 2. The He I line widths again show a very similar pattern to that of the Brγ, but are generally about 20% narrower. The deconvolved width is not a factor of two narrower as would be expected for purely thermal broadening. In LH96 it was found that a turbulent velocity component of 8.5 kms^{-1} was needed to explain the minimum width of the Brγ line and a similar value is required for the He I lines here. For more typical line widths seen in the HII region (24 kms^{-1} for HI, 20 kms^{-1} for HeI) and adopting the same temperature as in LH96 of 6500K, we find that a turbulent velocity of 10.5 kms^{-1} is required. Turbulent velocities in the range 8–18 kms^{-1} can explain all of the structure seen.

As expected the molecular hydrogen lines are much narrower although again not as narrow as for pure thermal broadening at around 100 K which would give a FWHM of only 0.5 kms^{-1} compared to the deconvolved width of the narrowest lines of about 5 kms^{-1}. Some turbulent component is almost certainly needed although this depends on how much of the velocity structure is due to global flows rather than local turbulence (see model later). The 5 kms^{-1} width is similar to that seen in NH_3 emission from hot clumps in VLA data (Cesaroni et al. 1994, 1998), and other dense molecular gas tracers such as CS and $C^{13}O$ (Churchwell, Walmsley & Wood 1992, Cesaroni et al. 1992) in G29.96−0.02 in larger beam radio and mm-wave observations. As in the ionized gas there is a very rapid increase in the line width ahead of the bow with signs of the molecular gas returning to a more quiescent state only at the last measured position of the on-axis data. A similar although less rapid increase in line width appears in the tail, again very similar to the ionized gas.

4 DISCUSSION

The advantage of these new data is the very accurate comparison of the velocity structure in the ionized and molecular gas. Along the axis of the cometary H II region the velocity difference between the ionized and molecular gas never exceeds about 4 kms^{-1}. In the bow shock model for this object (Van Buren & Mac Low 1992) it is predicted that most of the ionized gas emission should be redshifted relative to the ambient cloud as the exciting star bores its way into the molecular cloud and away from the observer. The maximum redshift should be the order of the star's relative velocity moderated by the cosine of the inclination angle or about 14 kms^{-1} in the Van Buren & Mac Low model. From our data this redshift is at most about 6 kms^{-1}.

In the tail region of G29.96−0.02 our data show strong evidence for a champagne flow with the ionized gas becoming progressively more blueshifted relative to the molecular gas. Moving into the main body of the nebula where the ionized gas is redshifted relative to the molecular gas we can understand this motion as expansion of the ionization front into the cloud behind (see Fig 5 of LH96 to help visualize the geometry of the object). The small amount of velocity structure in the molecular hydrogen emission through this main body region can also be understood as expansion. If the molecular hydrogen emission arises from a thin shell around the ionized zone that is already being set in motion by the expanding nebula then the observed velocity structure would result.

It is in the head region of the object where it becomes difficult to translate the observed velocity structure into any simple explanation or existing model. As one proceeds further into the head the ionized gas becomes progressively more and more blueshifted relative to the molecular gas. There are hints that the molecular gas begins to be dragged blue-wards as well before decoupling from the ionized gas at about the +5 arcsec offset along the on-axis position. Commensurate with the increasing blueshift of the ionized gas is a similarly dramatic increase in the line width. In a homogeneous flow picture this pattern in the line centroid and width has to be due to acceleration along the line of sight. Inspection of the geometry for G29.96−0.02, i.e. inclined at -135° (see Fig 5 of LH96), led us to explore the possibility of a substantial component of motion in the ionized gas tangential to the shell. Due to the orientation of the object tangential motion would be fully towards the observer in the head region whilst being tangential to the line of sight (and hence not observed) in the main body of the nebula. Physically this motion could be seen as a champagne flow where instead of the gas streaming straight along the axis of the object it is forced around the walls of the shell by the confining action of the stellar wind. An equivalent effect can be generated in the bow-shock model by adding gas pressure forces to the ram pressure ones they consider. Clearly, for lower stellar velocities, as we find here for G29.96−0.02, gas pressure forces play a more important role. However, in order to explain the increasing blueshift in the ionized gas we have to increase the speed of the tangential motion with distance from the shell. This seems to run against what one would expect physically. The tangential motion would accelerate from zero at the apex and so would naturally explain the large line widths along the line of sight in the head region.

In an attempt to quantify these ideas and test the expansion interpretation of the molecular hydrogen emission we have revamped the empirical model of LH96. The tangential motion described above was quantified by the form

$$v_{tan} = v_{tan}(max)(\phi/\pi)(l/l_{max})^{\alpha} \quad (1)$$

Hence the tangential component accelerates linearly with ϕ from the apex (ϕ=0) to the tail ($\phi \rightarrow \pi$). Ahead of the bow the velocity increases with the standoff distance l (l_{max} is the peak of the ionized shell). In order to attempt to match the on-axis data ahead of the bow an exponent α of at least two was necessary. However, if this was applied right around the object then the fit in the tail was very bad. Hence the exponent α was modulated such that

$$\alpha = 2(1 - \phi/\pi) \quad (2)$$

The model in LH96 also had a much sharper cut-off in density ahead of the bow than observations appear to show. Both K-band, Brγ and radio continuum images (LH96, Watson et al. 1997, Fey et al. 1995) all show emission extending away from the head at about the 10 per cent level for at least a couple of arcseconds. We suspect that there is some kind of partial ionization zone where ionizing photons are leaking into the dense gas ahead of the cometary region. To account for this we added an additional Gaussian shell component to the density distribution on the outside of the shell whose

peak density was three times lower than the main shell and whose width was ten times thicker. This provided a much better match to the flux distribution ahead of the bow.

Even after accounting for the partial ionization zone a purely tangential flow did not provide a good match to the observations. In particular the peak redshifted velocity occurred ahead of the peak flux rather than behind as in the data. We therefore included an expansion component as in the champagne model in LH96. The expansion was perpendicular to the shell, i.e. orthogonal to the tangential component and can be physically identified with expansion of the ionization front. In order not to produce line-splitting in the tail region the expansion velocity was modulated such that

$$v_{exp} = v_{exp}(max)(1 - \phi/\pi) \quad (3)$$

A model with v_{tan}(max)=20 kms^{-1} and v_{exp}(max)=20 kms^{-1} is compared with the observed Brγ flux, velocity centroid and width for both the on-axis and 6 arcsec off-axis positions in Fig 3. The essential features of the model can be seen in the on-axis velocity structure. Ahead of the apex at around +5 arcsec the tangential component means that the flow is coming towards the observer whilst the expansion component is mostly perpendicular to the line of sight. At the position of the star (0 arcsec) the situation is reversed and we see the expansion of the rear shell back into the molecular cloud. In the tail the flow becomes progressively more blueshifted as the gas accelerates towards us. The velocity field in the model over-predicts this blueshift, but further attempts to find a better empirical formalism were not felt to be warranted. A significant increase in the line width does occur in the head region for this model although still not enough to match the observations. The fit is still poor in the off-axis positions. Even so, the fact that there is a turnover in the velocity centroid is an improvement over the models in LH96.

We have developed a similar empirical model to investigate the molecular hydrogen velocity structure. The density distribution was assumed to have the same bow-type structure as the main ionized gas shell, but with a standoff distance l some 0.5 arcseconds larger. Since we believe the H_2 emission is mostly fluorescent we assumed the flux was proportional to density and the inverse square of the distance from the exciting star to take account of the geometric dilution of the UV radiation field. Fig 4 shows the results from such a model compared with the observed velocity structure. This model includes the same expansion component as did the model for the ionized gas with v_{exp}(max)=10 kms^{-1} , but has no tangential component to the motion. It gives a reasonable explanation for the motion in the main body of the nebula along the axis. Once again it cannot explain the broad widths ahead of the apex and the large amount of velocity structure off axis. The line widths in this model consisted of a thermal component with a temperature set at 100 K and a turbulent component of 3 kms^{-1}. This turbulent component is significantly less than that needed in the model of the ionized gas.

If the ionized and molecular hydrogen really do share the same type of expansion motion it would imply in a homogeneous scenario that molecular hydrogen arises from a thin shocked region ahead of the ionization front. The fact that the molecular gas is shocked does not of course mean that the observed H_2 emission is not dominated by fluorescence from the strong UV radiation field.

5 CONCLUSIONS

It is clear from our new data that the bow shock model proposed by Van Buren and Mac-Low (1992) is not a good match to the observations. We cannot rule out some supersonic motion of the star and its wind through the molecular cloud. Indeed, the velocity difference between the molecular hydrogen and the ionised gas tracers as a whole indicates that this relative motion is limited to less than 6 kms^{-1}. Therefore, this cannot explain the large 20 kms^{-1} velocity changes observed along the object. Furthermore, the evolution of the HII region around a slowly moving star is shown by Tenorio-Tagle, Yorke & Bodenheimer (1979). Clearly at late times any champagne flow element would dominate the expansion, so that the HII region would no longer be classified as ultracompact.

It is also equally clear that the classical champagne flow model we considered in LH96 is not a good match. The best fit we have found using a simple empirical model can be interpreted as a champagne flow model in which a powerful stellar wind influences the gas kinematics near the exciting star(s). Certainly the implied stellar type(s) of the exciting star(s) is consistent with the presence of such a wind. Watson et al. (1997) found that the exciting star should be at least 60 $M_\odot$ from JHK photometry (note, that the magnitudes we reported in LH96 for the exciting star(s) were in error: the correct values are K_n = 10.6, H= 12.1 and J= 14.6, and these are now consistent within the errors with the values reported by Watson et al).

Our new empirical model still fails to explain all the aspects of the observed data. In particular, two significant areas are left unexplained. First, the blueshifted emission ahead of the exciting star(s) and the fact that the lines becomes broader with increasing distance from the star. The former is perhaps indicative of a mass-loaded flow where clumping in the gas progressively randomizes the flow direction as it slows down. It is less easy to see why the velocity centroid shifts to the blue so rapidly. The other possible mechanism that in principle could explain both features is scattering. Henney (1998) describes a similar situation in which he explains broadened [OIII] emission in the Orion blister through scattering. Unfortunately, we cannot test this possibility with our current data. Secondly, the off-axis positions show a very similar velocity pattern to the on-axis one. The discrepancy between the model and the off-axis positions probably simply reflects the limits of our empirical model rather than anything more complex however.

In summary then, it seems clear that the dominant mechanism determining the kinematics in G29.96−0.02 is a combination of a reasonably normal champagne flow channelled into a thin shell by the stellar wind.

ACKNOWLEDGEMENTS

The United Kingdom Infrared Telescope is operated by the Joint Astronomy Centre on behalf of the Particle Physics and Astronomy Research Council and we are grateful for

the support given during the observations. We would like to thank Dave van Buren for valuable discussion on the relative merits of bow-shock and champagne flow models for this source, and Alan Watson for highlighting the difference between our previously published photometry for the exciting star and his own.

References

Bashkin S., Stoner J.O., 1975, Atomic Energy Levels and Grotrian Diagrams, North Holland Publishing Company, Amsterdam
Bragg, S.L., Brault, J.W., Smith, W.H., 1982, ApJ, 263, 999
Cesaroni, R., Walmsley, C.M., Kompe, C., Churchwell, E., 1992, A&A, 253, 278
Cesaroni, R., Churchwell, E., Hofner, P., Walmsley, C.M., Kurtz, S., 1994, A&A, 288, 903
Cesaroni, R., Hofner, P., Walmsley, C.M., Churchwell, E., 1998, A&A, 331, 709
Churchwell, E., Walmsley, C.M., Wood, D.O.S., 1992, A&A, 253, 541
Dyson, J.E., Williams, R.J.R., Redman, M.P., 1995, MNRAS, 277, 700
De Pree, C.G., Rodriguez, L.F., Goss, W.M., 1995, RmxAA, 31, 39
Fey, A.L., Gaume, R.A., Claussen, M.J., Vrba, F.J., 1995, ApJ, 453, 308
Fich M., 1993, ApJS, 86, 475
Henney, W.J., 1998, ApJ, 503, 760
Hollenbach, D., Johnstone, D, Lizano, S., Shu, F., 1994, ApJ, 428, 654
Hofner, P, Churchwell, E., 1996, A&AS, 120, 283
Icke V., Gatley I., Israel F. P., 1980, ApJ, 236, 808
Israel F. P., 1978, A&A, 90, 769
Kurtz S., Churchwell E., Wood D. O. S., 1994, ApJS, 91, 659
Lumsden, S.L., Hoare, M.G., 1996, ApJ, 464, 272
Mac Low M.-M., Van Buren D., Wood D. O. S., Churchwell E., 1991, ApJ, 369, 395
Oliva E., Origlia L., 1992, A&A, 254, 466
Redman, M.P., Williams, R.J., Dyson, J.E., 1996, MNRAS, 280, 661
Redman, M.P., Williams, R.J., Dyson, J.E., 1998, MNRAS, 298, 33
Tenorio-Tagle, G., Yorke, H.W., Bodenheimer, P., 1979, A&A, 80, 110
Van Buren D., Mac Low M.-M., 1992, ApJ, 394, 534
Watson, A.M., Coil, A.L., Shepherd, D.S., Hofner, P., Churchwell, E., 1997, ApJ, 487, 818
Williams, R.J.R., Dyson, J.E., Redman, M.P., 1996, MNRAS, 280, 667
Wood D. O. S., Churchwell E., 1989, ApJS, 69, 831
Yorke, H.W., 1986, ARA&A, 24, 49

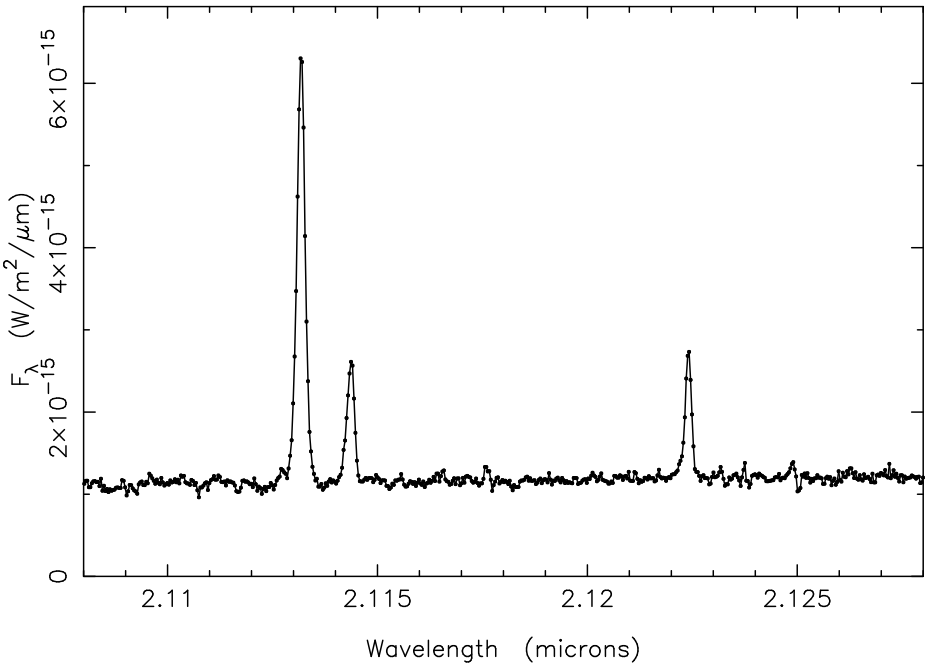

Figure 1: Extracted spectrum of G29.96−0.02 for a 1 arcsecond by 4.5 arcsecond region around the flux peak. The lines are (from left to right) the 4^3S–3^3P and 4^1S–3^1P transitions of HeI, and the 1–0 S(1) transition of H_2. The absolute flux calibration is only approximate.

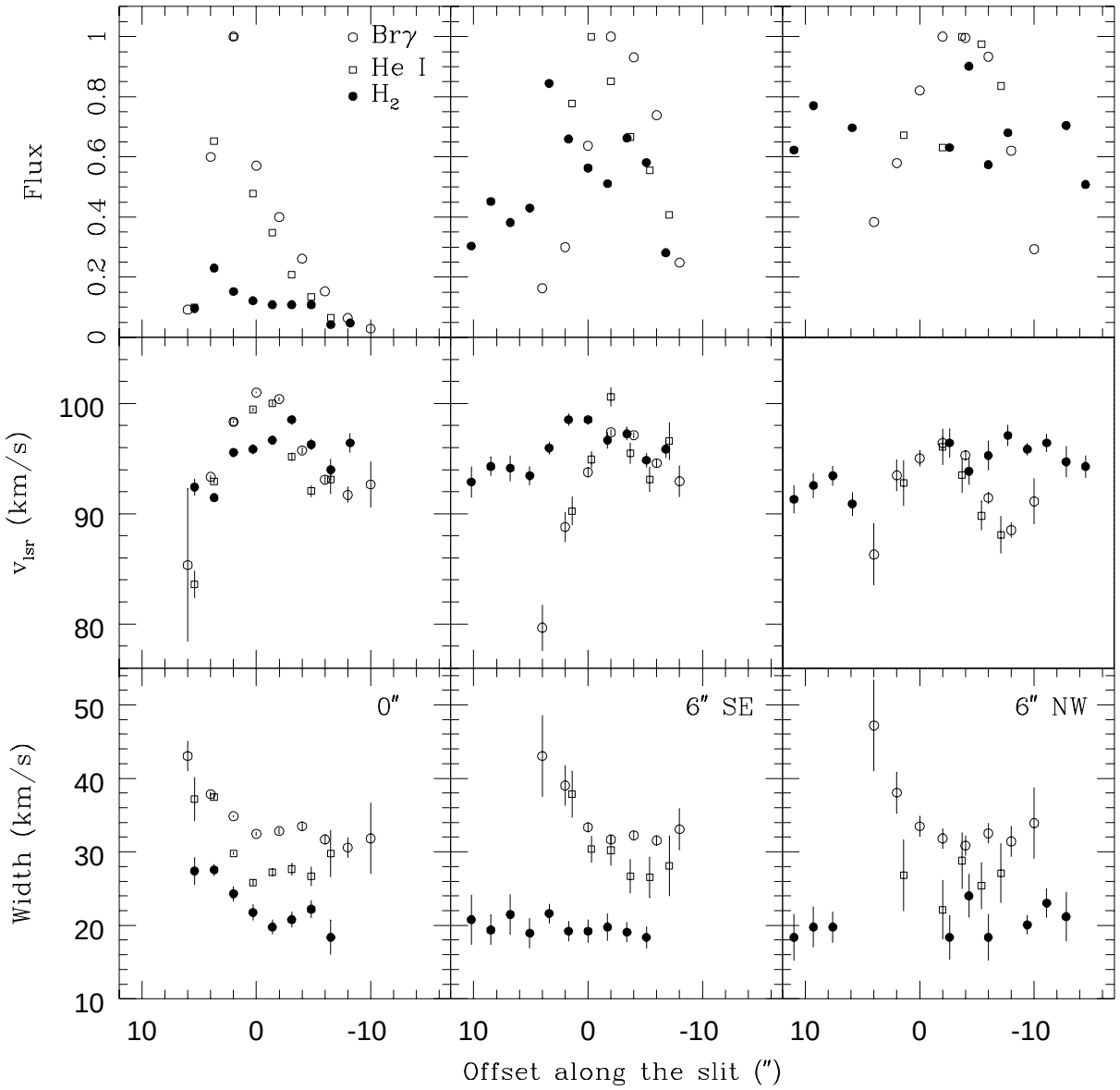

Figure 2: Comparison of the observed flux, velocity centroid and line width along the slits for the three lines Brγ He I and 1-0 S(1) H_2. The three different vertical panels show the results for the three different slit positions - on the axis of the object, 6 arcseconds to the SE and 6 arcseconds to the NW. The Brγ and He I fluxes are normalized and their spatial profiles agree well as expected. The 1-0 S(1) H_2 flux is shown relative to the Brγ flux. The zero offset along the slit corresponds to the position of the exciting star.

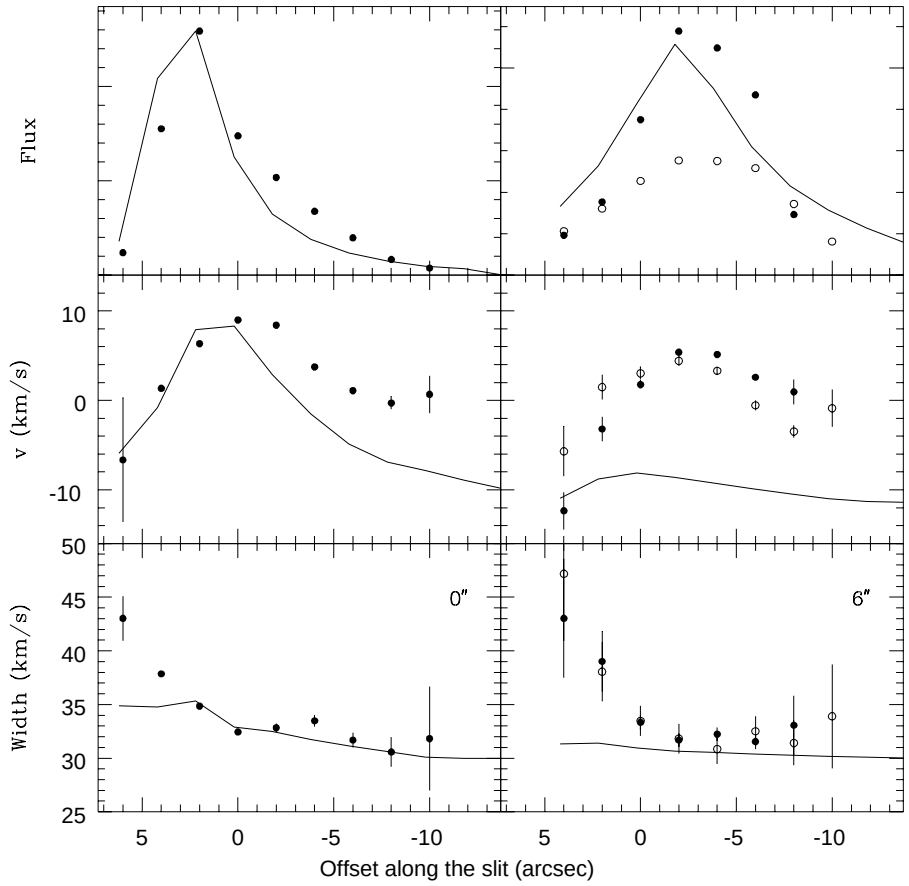

Figure 3: Comparison of the empirical model (solid line) for the ionized gas with the Brγ data (points). In the right hand panel the solid circles are the 6 arcsec SE data and the open circles are the 6 arcsec NW data. The model flux has been normalized to the peak flux of the on-axis data. The velocities are now with respect to the undisturbed ISM (or star); a v_{lsr}=92 kms^{-1} has been subtracted from the data.

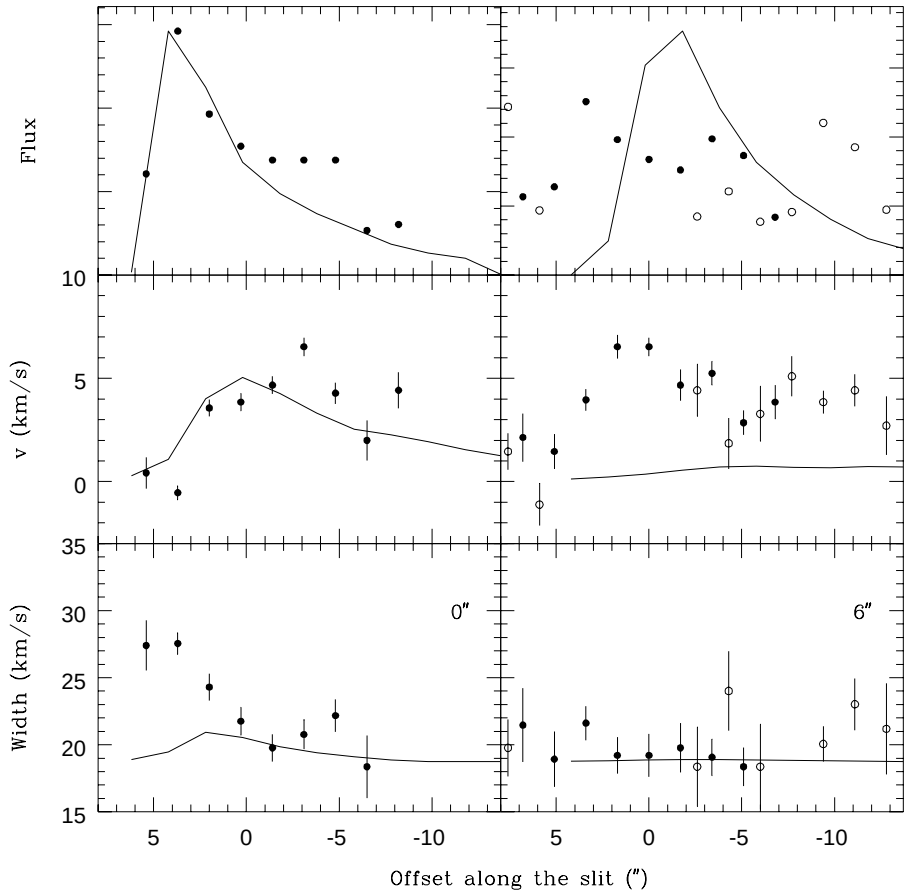

Figure 4: Comparison of the empirical model (solid line) for the molecular gas with the H_2 data (points). A v_{lsr}=92 kms^{-1} has also been subtracted from the observed velocities.